

Data diversity and virtual imaging in AI-based diagnosis: A case study based on COVID-19

Fakrul Islam Tushar, Lavsen Dahal, Saman Sotoudeh-Paima, Ehsan Abadi, W. Paul Segars, Ehsan Samei, Joseph Y. Lo

Center for Virtual Imaging Trials,
Carl E. Ravin Advanced Imaging Laboratories,
Dept. of Radiology, Duke University School of Medicine
Dept. of Electrical & Computer Engineering, Pratt School of Engineering, Duke University

Abstract

Many studies have investigated deep-learning-based artificial intelligence (AI) models for medical imaging diagnosis of the novel coronavirus (COVID-19), with many reports of near-perfect performance. However, variability in performance and underlying data biases raise concerns about clinical generalizability. This retrospective study involved the development and evaluation of artificial intelligence (AI) models for COVID-19 diagnosis using both diverse clinical and virtually generated medical images. In addition, we conducted a virtual imaging trial to assess how AI performance is affected by several patient- and physics-based factors, including the extent of disease, radiation dose, and imaging modality of computed tomography (CT) and chest radiography (CXR). AI performance was strongly influenced by dataset characteristics including quantity, diversity, and prevalence, leading to poor generalization with up to 20% drop in receiver operating characteristic area under the curve. Model performance on virtual CT and CXR images was comparable to overall results on clinical data. Imaging dose proved to have negligible influence on the results, but the extent of the disease had a marked affect. CT results were consistently superior to those from CXR. Overall, the study highlighted the significant impact of dataset characteristics and disease extent on COVID assessment, and the relevance and potential role of virtual imaging trial techniques on developing effective evaluation of AI algorithms and facilitating translation into diagnostic practice.

Introduction:

For effective development and optimization, artificial intelligence (AI) models typically require massive amounts of data. In medical imaging, acquiring patient data is very difficult and annotation can be very time-consuming and subject to reader variability. As a result, even with advanced algorithms trained extensively on large datasets, AI models often struggle to generalize, resulting in limited clinical applicability. Consider the context of the early stages of the COVID-19 pandemic, when chest radiography (CXR) and computed tomography (CT) were widely employed for detecting and managing lung infections.^{1,2} Given the global urgency surrounding COVID-19, researchers rushed to develop AI aides for radiologists, but many studies reported unrealistic, near-perfect results that dropped significantly almost to chance upon external testing.³⁻⁹ In the field of medical imaging, failure of AI deep learning models to generalize is a pervasive problem. There is a pressing need for an evaluation framework that can assess if the performance of imaging models can truly generalize. When they fail to generalize, we need to understand what out-of-distribution factors (e.g., patient normal anatomy and disease, or imaging physics conditions) are driving the model performance.

To enhance the robustness of machine learning models, numerous public datasets containing CXR and CT images were released.¹⁰⁻¹⁷ Although they vary in quantity and quality, most datasets lacked representative characteristics for technology and patients. An ongoing large effort has been led by the Medical Imaging and Data Resource Center (MIDRC).¹⁸ To date, although a plethora of models were proposed, biases and uncertainties in the underlying data fundamentally limit performance generalizability.^{17,19-24} A review of 62 studies on AI image diagnosis of COVID-19 asserted that none of these models were fit for clinical use due to methodological flaws and underlying biases.¹⁷ The lack of careful controls in the clinical data also precluded further analysis for model explainability.

A promising solution to this challenge lies in the use of the virtual imaging trial (VIT) approach, which simulates three key components of an imaging trial: patients, scanners, and readers.²⁵ VITs provide practical opportunities to quantify the effects of imaging technologies and patient factors on radiological diagnosis. VITs allow the controlled comparison of alternative imaging modalities or the optimization of acquisition protocols. Previously, the VIT approach was demonstrated for COVID-19 using computational anatomical model of patients with and without COVID-19 pneumonia in simulated CT scans.^{26,27} In particular, a VIT framework can generate virtual patients and scans with pixel-level ground truth to serve as a truly independent external validation set to evaluate AI models. Furthermore, by

simulating a range of imaging technologies and patient characteristics, the VIT approach makes it possible to evaluate which factors are driving model performance.

Previously, we performed external validations of open-source deep-learning models for COVID-19 classification with CT and CXR images.^{28,29} The current study builds upon that prior work by including simulated CT and CXR exams from the same virtual patients at effective doses ranging over multiple orders of magnitude that overlapped between the two modalities. Augmented with twice as many clinical datasets and multiple AI models compared to the prior study, we aimed to unpack the interplay of dataset-model matching and mismatching on the results, a comparison of model performance on virtual and clinical data, a systematic assessment of CT and CXR from the same cases, and the influence of patient- and physics-based factors on the generalizability of the results.

Results:

Study design and overview. Institutional Review Board approval was obtained for this exempt study that used only anonymized image data and simulated phantom data. We briefly outline our study design that is necessary to understand the experimental results and analysis.

Multiple light-weight convolutional neural network (CNN) models with residual connections were developed to process CT or CXR images to classify cases as positive or negative for COVID-19. Multiple clinical datasets were acquired,^{10,12-14,16,21,30-33} which vary in size, diversity, demographics, and class definitions. In addition, we simulated image data from a population of 4D-XCAT models with varying COVID-19 size and distribution, developed in a previous study then generating images using virtual CT and CXR scanners (DukeSim, CVIT, Duke University)²⁶. The CNN models were trained using single and various combinations of clinical datasets. In parallel experiments, CT or CXR clinical data were analyzed for internal and external performance shift. The simulated data were reserved as a separate external validation. Finally, by varying the virtual imaging trial parameters, we explored how performance may be affected by factors pertaining to the patients (i.e., infection size) or imaging physics (i.e., effective dose and modalities). An illustration of the overall workflow of the analysis is presented in Fig. 1.

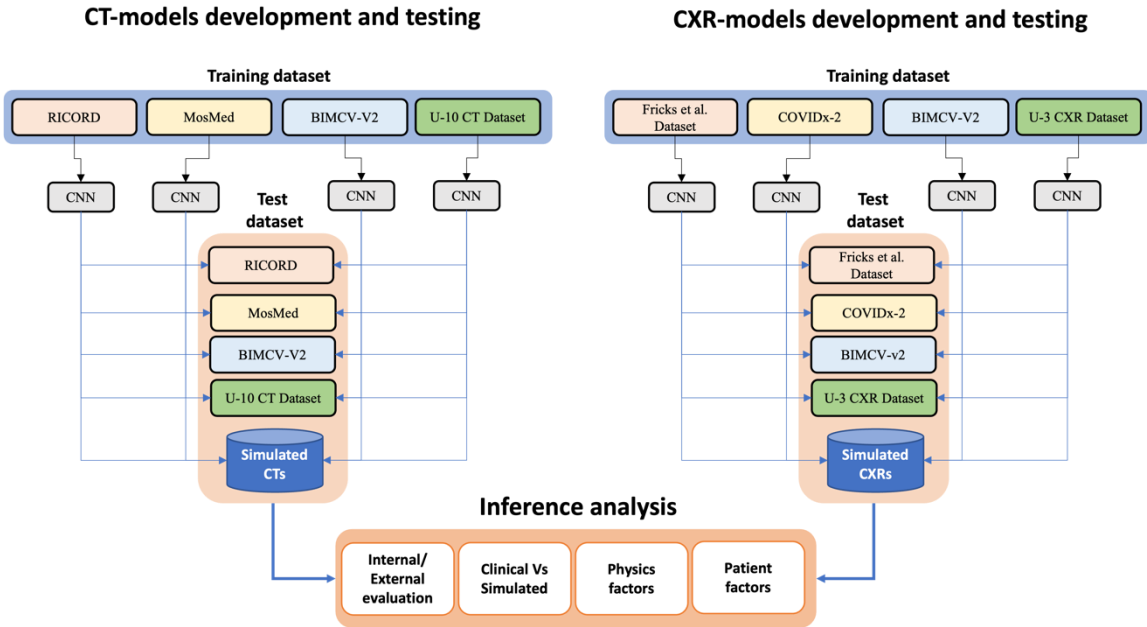


Figure 1. Study design overview. 12,844 CT scans and 25,219 CXR images for COVID-19 diagnosis were drawn from 13 clinical datasets comprising single or multiple centers (Supplement Fig. 1-2). Multiple deep-learning-based models were developed using these clinical datasets. All models underwent internal testing (held-out from the same training dataset) and external testing (all other datasets). Further external testing was performed using virtually simulated CT and CXR images to analyze effect of patient and imaging physics factors.

Clinical dataset construction. The clinical CT data included a total of 12,844 volumes of 7,452 patients from 10 datasets: RICORD,¹⁶ MosMed,¹³ BIMCV-COVID-19 +/- (BIMCV-V2),¹² COVID-CT-MD,¹⁰ CT Images in COVID-19,¹¹ Plethora,³³ COVID19-CT-dataset,³⁰ Stony Brook University COVID-19 Positive Cases (COVID-19-NY-SBU),¹⁴ A Large-Scale CT and PET/CT Dataset for Lung Cancer Diagnosis (Lung-PET-CT-Dx),³¹ and Lung Image Database Consortium / Image Database Resource Initiative (LIDC-IDRI).³⁴ These datasets had different prevalence of COVID-19 positive and negative images (Supplement Fig. 2a) and demographics. Summary statistics regarding the datasets are detailed in Table 1.

Furthermore, all ten clinical CT datasets above were combined to create the U-10 CT dataset, which provides a more diverse dataset for factors such as patient population and demographics, disease appearances, CT systems, and imaging protocols. Supplement Fig. 1 shows the inclusion and exclusion criteria followed in the curation of the clinical CT data.

CXR analysis included 25,219 clinical CXR images collected from 3 datasets: Fricks et al.,²¹ BIMCV,¹² and COVIDx-CXR-2.³² These datasets also had different prevalence of COVID-19 positive and negative images (Supplement Fig. 2b) and demographics.

All three clinical CXR datasets were also combined to form the U-3 CXR dataset. In one of the datasets, COVIDx-CXR-2, positive images were from different sources, but the negative class was much larger and mainly from one source, namely the RSNA Pneumonia Detection Challenge³⁵ (Supplement Fig. 2b). For better balance when training and validating the unified U-3 dataset, the negative cases were randomly subsampled to balance the two classes equally. However, COVIDx-CXR-2 specified a particular test set which was used unaltered in all the experiments. Summary statistics regarding the CXR datasets are detailed in Table 2.

Virtual dataset construction. Simulated CT and CXR datasets were generated in three steps using a virtual imaging trial (VIT) framework.^{25,26} First, XCAT computational phantoms were designed to include structures of normal anatomy. Second, diseased regions of COVID-19 pneumonia were segmented, computationally modeled, and inserted within the lungs. Finally, these virtual patient models with or without the disease were imaged using an x-ray image acquisition simulator (DukeSim, CVIT, Duke University).^{26,27} Virtual scans were repeated at different effective doses (0.01, 0.1, 0.3, 1.6, 5.6, and 11.2 mSv). The dose settings were selected to represent a wide range of clinical applicability, as well as direct comparison of CT and CXR images at the same hypothetical dose. For the CXR acquisitions, two commercial post-processing algorithms (denoted as Algorithm A and B to maintain confidentiality) were applied to examine the effects of vendor heterogeneity.

Table 3 shows the characteristics of the generated CT and CXR images. Supplement Table 1 details the unique attributes of simulated CT and CXR images compared to the curated clinical datasets.

Model development and training. To minimize overtraining, we intentionally selected lightweight ResNet-like models^{36,37} (Supplement Fig. 3) and trained four separate CT-based models using the RICORD, MosMed, BIMCV, and U-10 CT datasets. Similarly, for CXR, we trained four different EfficientNetv2³⁸ models using the data from Fricks et al., BIMCV, COVIDx-CXR-2, and U-3 CXR datasets, respectively. Each dataset was randomly divided by patient into subsets of training (60%), validation (20%), and testing (20%). As we aimed to assess the utility of virtual data to assess clinically trained algorithms, for virtual data, no training was applied – the model as trained by clinical data was applied to the entire dataset for testing.

The clinical datasets were selected to encompass a range of study samples. Specifically, limited datasets included RICORD for CT and Fricks et al. for CXR, while U-10 CT and U-3 CXR were more diverse. Detailed descriptions of the models and training processes can be found in the Methods (Fig. 1).

Evaluation and statistical analysis. We conducted a series of studies to assess the model performance on clinical datasets and on virtual datasets. For the virtual dataset, we further evaluated the influence of physics factors, i.e., the imaging modality and the acquisition effective dose. We additionally evaluated the effect of the patient factor of infection size, wherein the simulated COVID-19 pneumonia cases were divided into two groups: "higher" infection (above the median value of 2.6% of total lung volume) and "lower" infection (below this median value). All performances were evaluated using the receiver operating characteristic area under the curve (AUC) with 95% confidence interval (CI) calculated by the DeLong method as implemented by pROC 1.16.2 in R 3.6.1 with 2000 bootstrapping samples.³⁹

Evaluation of the models on clinical datasets. As depicted in Fig. 2, clinical CT and CXR models exhibited a consistent drop in performance from internal to external testing, and those differences often exceeded the confidence intervals. The CT models showed an internal validation AUC range of 0.69 to 0.85, whereas external testing consistently dropped to between 0.54 and 0.76. Similarly, for CXR models, internal performance ranged from AUC of 0.77 to 1, while external testing AUC again dropped to a range of 0.51 to 0.73. Models trained on the most diverse datasets (U-3 CXR and U-10 CT) consistently yielded a testing performance that was the highest or second highest. Notably, in spite of its size, the COVIDx-CXR-2 dataset for CXR was very biased, resulting in perfect internal validation and near-perfect external testing even for the U-3 model that was trained on all three datasets.

Evaluation of the models on virtual datasets. As shown in Fig. 2, compared to clinical data, all CT models performed consistently with intermediate AUC values on these simulated data, which suggests they may be less biased. Among the CT models, training with the most diverse U-10 CT dataset yielded the highest testing performance on the simulated CT images. Conversely, all CXR models displayed comparably poor performance on the simulated CXR images.

Patient-based evaluation. Assessing the effect of infection size on the performance of models, Fig. 3 shows all models performed better on both CT and CXR images with higher infection compared to images with lower infections.

Acquisition-based evaluation: For the same virtual patients, we assessed the performance of models over a wide, overlapping range of effective doses for the virtual CT and CXR acquisitions. As shown in Fig. 4, the 3D CT models consistently outperformed the 2D CXR models, but the confidence intervals for the AUCs overlapped. Within each modality, although the effective dose (mSv) varied by 30-fold to represent the widest possible range of clinical use, there was no statistically significant change in performance.^{40,41}

Table 1. Clinical CT patient datasets utilized in model development and testing. The combination of all ten constitutes the U-10 CT dataset. Demographic values are reported as the percentage of patient sex and mean of patient age.

No	Dataset	Source	Demographics	Train*	Validation*	Test*
1.	RICORD ¹⁶ (1b,1b)	Turkey, USA, Canada, Brazil	44% women Age 54 ±17	136 (162)	45 (55)	46 (58)
2.	MosMed ¹³	Russia	56% women Age 47	664 (664)	220 (220)	226 (226)
3.	BIMCV-V2 ¹²	Spain	42% women. Age 64 ±16	1183 (3498)	391 (1190)	420 (129)
4.	COVID-CT- MD ¹⁰	Iran	40% women. Age 51 ±16	182 (182)	60 (60)	63 (63)
5.	An et al. dataset ¹¹	Multi- center	N/A	379 (391)	126 (129)	127 (130)
6.	Plethora ³³	USA	31% women. Age 68 ± 10	241 (241)	80 (80)	81 (81)
7.	COVID19- CT ³⁰	Iran	39.1% women Age: 47 ± 16	604 (604)	201 (201)	202 (202)
8.	COVID-19- NY-SBU ¹⁴	USA	43% women. (Age: ranges between 18-90 years)	251 (739)	84 (278)	84 (282)
9.	Lungs-CT- Dx ³¹	China	46% women, Age 61 ± 10	207 (479)	69 (154)	70 (164)
10.	LIDC- IDRI ³⁴	USA	N/A	606 (611)	202 (204)	202 (203)
Total / U-10 CT				4453 (7571)	1478 (2571)	1521 (2702)

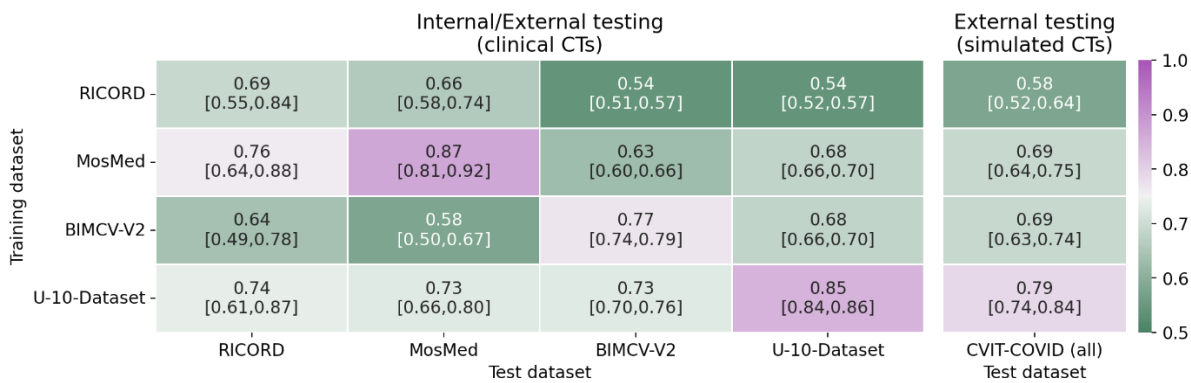
Note-* Number of patients (number of scans), COVID-19-NY-SBU = Stony Brook University COVID-19 Positive Cases, Lungs-CT-Dx= A Large-Scale CT and PET/CT Dataset for Lung Cancer Diagnosis

Table 2. Clinical CXR Patient Cohorts utilized in model development and testing. Demographic values are reported as the percentage of patient sex and mean of patient age.

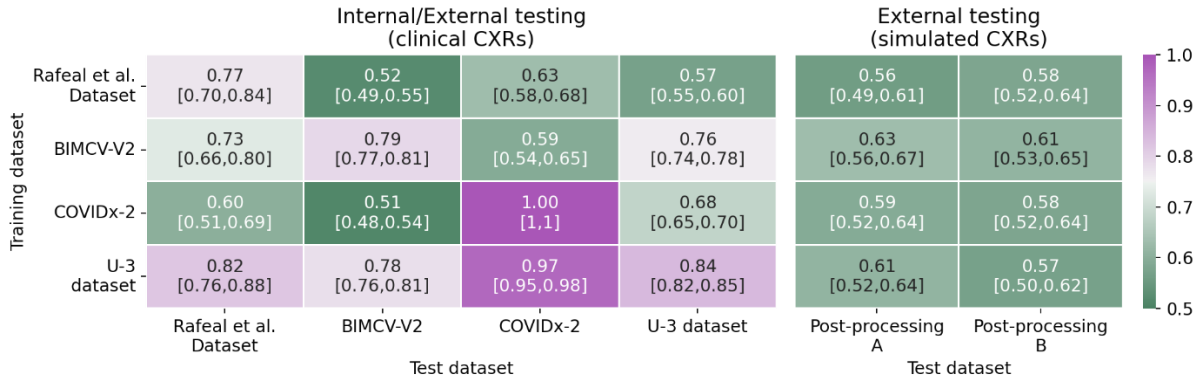
No	Dataset	Source	Demographics	Train	Validation	Test
1.	Fricks et al. ²¹	Iran, Italy, USA	N/A	718	180	226
2.	BIMCV-V2 ¹²	Spain	46% Women Age 63 ± 17	4959	1240	1551
3.	COVIDx-CXR- 2 ³²	Multi-center	N/A	12761	3190	400
	Total		N/A	18438	4610	2177
4	U-3 CXR dataset		N/A	9930	2482	2177

Table 3. Simulated (CVIT-COVID) dataset.

Effective dose (mSv)	Number of virtual exams*		
	COVID-19		Negative
	CVIT-COVID-CT		
0.3	50		40
1.6	50		40
5.6	50		40
11.2	50		40
Total (CT)	200		160
CVIT-COVID-CXR			
0.01	50		40
0.10	50		40
0.3	50		40
Total (CXR)	150		120

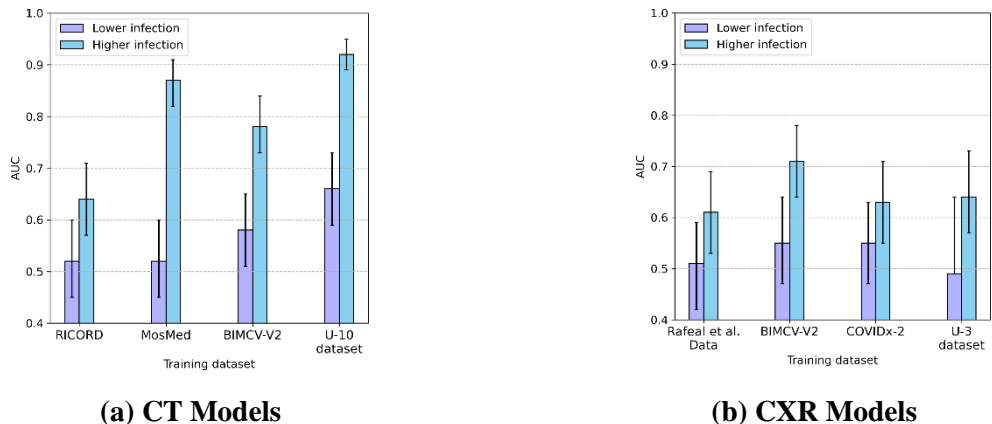


(a) CT Models



(b) CXR Models

Figure 2. Confusion matrix of COVID-19 classification performance of (a) CT and (b) CXR models. Training dataset is shown in rows and testing dataset in columns; diagonal represents internal validation, while off-diagonal entries are external testing. Additional external testing on simulated images is shown on the right. Performance is reported as receiver operating characteristic area under the curve with 95% confidence interval. All models generally performed worse on external testing with both clinical and simulated data. However, models trained with the union datasets (U-10 CT and U-3 CXR) consistently yielded the highest external testing performance. Furthermore, simulation testing consistently provided intermediate results that may be more indicative of true performance.



(a) CT Models

(b) CXR Models

Figure 3. Both (a) CT and (b) CXR models each trained on four datasets (represented on the x-axis), consistently demonstrated superior performance in "higher infection" cases, where the pneumonia volume exceeded the median, compared to "lower infection" cases that fell below the median. For CXR, results were almost identical for the two post-processing algorithms, so only algorithm A is shown. Error bars represent the 95% confidence interval.

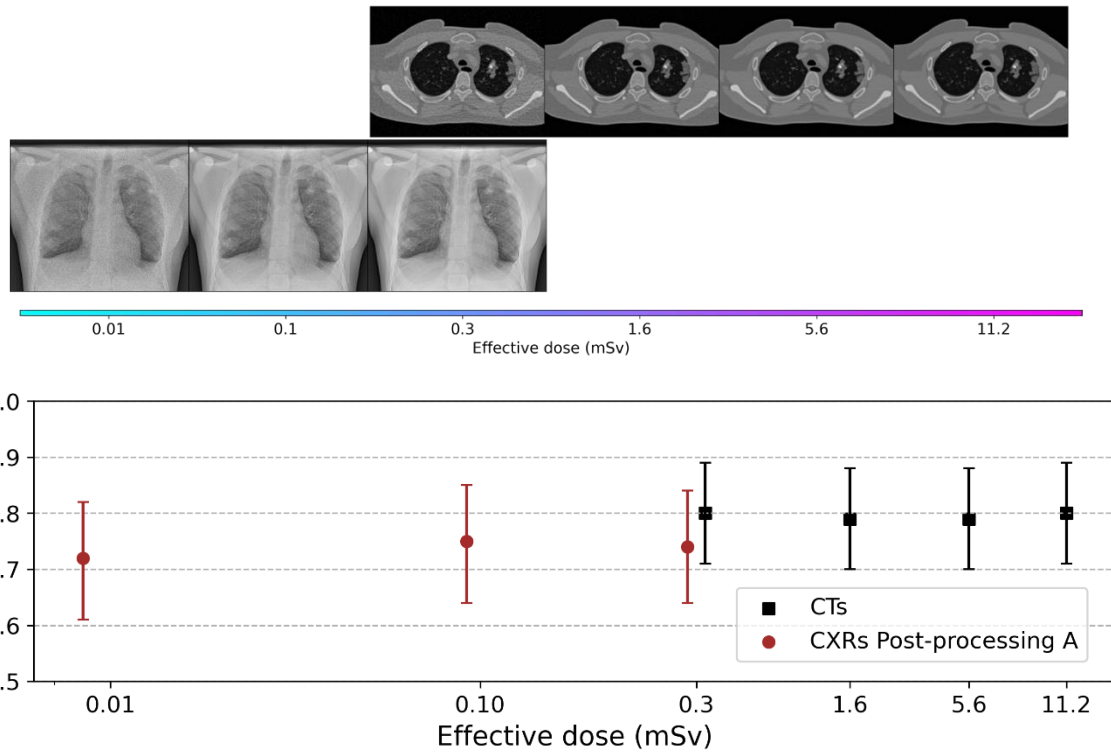


Figure 4. Simulated images were used to evaluate physics-based factors. Although models consistently performed better on CT over CXR, the differences were not significant at the shared dose of 0.3 mSv. Within each modality, performances were also not significantly different across a wide range of effective dose. Error bars correspond to 95% confidence interval.

Discussion:

There has been considerable research to develop AI models to improve radiology diagnosis. However, practical application of these models in clinical practice has been hindered by two related challenges. First, models often underperform when applied to a new dataset with different attributes such as patient demographics, acquisition protocols, or scanner vendor. Second, most models function as “black boxes” that lack interpretability, making it difficult to determine which factors account for the poor performance. These issues became particularly evident during the urgent scientific response to COVID-19, when many early studies reported high performances that did not generalize.^{19,22,24,28,29,42} Although biases in AI models for healthcare may be unavoidable, a comprehensive understanding of such factors, supported by effective external testing, can raise the confidence that such models can be deployed effectively and responsibly.^{17,19,43} This study addresses the problem of biases in medical imaging AI models by

leveraging clinical and simulated data for independent testing, thus enabling the evaluation of both generalizability and interpretability.

We compiled a large cohort of clinical CT and CXR images from dataset resources representing over 22,000 patients. In spite of the large amount of training data, however, model performance was still impaired due to class imbalance and confounding issues such as radiographic markers, incorrect image orientation, and collimator edges.^{19,24,44} Proper data curation is time consuming and requires domain expertise in medical imaging, rendering this process prohibitively costly.⁴⁵ Therefore, external validation of AI models is essential to rule out biases.^{17,19} To address these needs, this study utilized a VIT simulation platform.^{25,26} Using simulated CT and CXR images provides two crucial advantages. First, simulated image data enables external validation that is not only truly independent but also controlled. Second, the VIT framework allows evaluating the models under different patient- and physics-based factors, which offers interpretability and reveals clinical or technical insights. VIT simulations facilitate conducting medical imaging studies in a trustworthy, reproducible, and practicable manner.

Our primary objective was to analyze the impact of dataset variability on model development. Unlike most studies, we intentionally chose to use very lightweight networks to minimize overfitting.^{36,37} Nevertheless, all models still dropped in performance substantially from internal to external testing, which was in line with previously-reported studies.^{19,24,28,29} Since model performance reflects the underlying data, this generalizability gap suggests the lack of diversity in the existing datasets with regard to institution bias, patient demographics, disease appearances, and image quality.^{19,22,44} To minimize such bias, we trained on the combination of multiple diverse datasets, U-10 CT and U-3 CXR, and the resulting models outperformed the single-dataset models in independent testing. The model trained on the diverse U-10 CT dataset demonstrated very consistent performance across all three clinical datasets with an AUC of approximately 0.73. Unlike the individual testing results showing considerable high and low bias, this moderate result is more credible and may indicate a more representative performance for this challenging clinical task. These general trends were also observed for the CXR datasets but with considerable residual bias due to the disproportionate influence of the COVIDx-CXR-2 dataset, which is much larger than other datasets and leads to confounding bias as its positive and negative cases come from different institutions. This quandary shows that despite rigorous training and external testing, AI models can still be affected by fundamental data biases.

The VIT process proved to deliver a more realistic portrayal of true clinical performance. When the many models were tested on simulated images, performances fell consistently within the middle of the range of

external testing on clinical datasets, suggesting that the simulations presented data with an appearance that was realistic and relevant. This is highly encouraging considering the models were applied to the virtual data without even being trained on them, highlighting the potential generalizability of virtual dataset to evaluate AI-based diagnosis algorithms. Unlike clinical datasets, the simulated images are further free of institutional bias or other confounding factors, because the VIT framework offered precisely reproducible controls in terms of patient sampling as well as physical image formation. This enabled us to compare identical virtual patients with and without COVID-19, and also to conduct virtual imaging of each patient using both CT and CXR. The degree of experimental control provided by VITs is not physically possible in real clinical trials.

Our VIT analysis further provided intriguing insights into the effects of patient- and physics-based factors driving AI performance. Regardless of the training datasets for both the CT and CXR models, there was a noticeable increase in performance when the COVID-19 infection size was larger than the median value. For both imaging modalities, performances stayed consistent even across a 30-fold range in effective dose (which well exceeds the range in clinical practice), suggesting that dose may not be as relevant for the AI detection of diffuse diseases such as pneumonia. In stark contrast to the model evaluation on clinical data, our analysis confirmed that CT outperformed CXR, which was consistent with expectations since 3D CT scans provide superior spatial information over 2D CXR images.

This study had several limitations. Although the simulated CT and CXR images realistically reproduced both anatomical and physical processes, they were generated from a pool of fifty virtual patients with variable anatomy and severity of the disease. Consequently, simulation testing showed consistent trends but with large confidence intervals. Future work will increase the number of computational phantoms to represent even larger and more diverse patient populations. In terms of the network architectures, each modality was analyzed using a single lightweight design, foregoing extension experiments with other networks. Models were developed only to conduct case-level classification, which is the only annotation available in almost all datasets. Furthermore, the label of COVID-19 as negative or positive was defined by each dataset, and those standards varied widely, including radiologist assessment or different diagnostic tests.¹ Some datasets included both COVID-19 pneumonia and other types of pneumonia, which may not be readily differentiated by imaging alone.

Conclusions:

AI-based diagnosis models hold the potential to revolutionize healthcare. However, factors contributing to model bias remain underexplored, especially in the medical imaging domain. An essential prerequisite to clinical deployment is a robust external evaluation. Virtual imaging trials can meet that need by providing the necessary image data that is objective and controlled. By studying patient- or physics-based factors influencing model performance, these procedures also offer interpretability and opportunities for model refinement. Through these contributions, virtual imaging trials can enhance clinical trials, making them faster, more rigorous, and more reproducible.

Methods:

Preprocessing. Before classification, standard preprocessing was performed on both CT and CXR images. Each CT volume was resampled to voxel dimensions of $2 \text{ mm} \times 2 \text{ mm} \times 5 \text{ mm}$ (w, h, d). Intensities were clipped between -1000 to 500 HU, then standardized to mean of 0 and standard deviation of 1. To reduce computational cost and the influence of background organs, three-dimensional (3D) patches of size $160 \times 160 \times 96$ (w, h, d) were centered about the lungs. The patch size was based on average lung size plus a margin to allow for patient variability. CXR images were resized and randomly cropped to a size of 300x384 pixels, then standardized to 0.5 mean and 0.5 standard deviation to maintain consistency with the pre-trained dataset.

Model training details. CT models used a simple 3D CNN inspired by ResNet;⁴⁶ the architecture is shown in Supplement Fig. 3. After initial convolution, features were learned across two resolution scales, then halved by max-pooling (pooling size $2 \times 2 \times 2$) while doubling the number of filters. The last R-block features underwent batch normalization, rectified linear unit (ReLU), global max-pooling, dropout (dropout rate 0.5), and finally a dense classification layer with sigmoid activation for binary classification. The stochastic gradient descent (SGD) optimizer was used to optimize the weights with decay learning rate, and weighted binary cross-entropy was used as the loss function. Weights were initialized to a uniform distribution. To retain the natural prevalence, no class-balancing was performed during training. CXR models were based on Efficientnetv2 with the original architecture.³⁸ SGD was selected as the optimizer with the learning rate scheduler,⁴⁷ initial learning rate of 0.01, and cross-entropy loss. All models were developed using Python TensorFlow v2.6 and PyTorch deep learning frameworks. All model weights, initial hyper-parameters, and code will be publicly accessible at <https://gitlab.oit.duke.edu/cvit/>.

References:

- 1 Rubin, G. D. *et al.* The Role of Chest Imaging in Patient Management during the COVID-19 Pandemic: A Multinational Consensus Statement from the Fleischner Society. *Radiology* **296**, 172-180 (2020).
- 2 Kanne, J. P. *et al.* COVID-19 Imaging: What We Know Now and What Remains Unknown. *Radiology* **299**, E262-E279 (2021).
- 3 Gunraj, H., Wang, L. & Wong, A. COVIDNet-CT: A Tailored Deep Convolutional Neural Network Design for Detection of COVID-19 Cases From Chest CT Images. *Front Med (Lausanne)* **7**, 608525 (2020).
- 4 Harmon, S. A. *et al.* Artificial intelligence for the detection of COVID-19 pneumonia on chest CT using multinational datasets. *Nat Commun* **11**, 4080 (2020).
- 5 Javaheri, T. *et al.* CovidCTNet: an open-source deep learning approach to diagnose covid-19 using small cohort of CT images. *NPJ Digit Med* **4**, 29 (2021).
- 6 Jin, C. *et al.* Development and evaluation of an artificial intelligence system for COVID-19 diagnosis. *Nat Commun* **11**, 5088 (2020).
- 7 Bai, H. X. *et al.* Artificial Intelligence Augmentation of Radiologist Performance in Distinguishing COVID-19 from Pneumonia of Other Origin at Chest CT. *Radiology* **296**, E156-E165 (2020).
- 8 Afshar, P. *et al.* COVID-CAPS: A capsule network-based framework for identification of COVID-19 cases from X-ray images. *Pattern Recognition Letters* **138**, 638-643 (2020).
- 9 Panwar, H., Gupta, P. K., Siddiqui, M. K., Morales-Menendez, R. & Singh, V. Application of deep learning for fast detection of COVID-19 in X-Rays using nCOVnet. *Chaos, Solitons & Fractals* **138**, 109944 (2020).
- 10 Afshar, P. *et al.* COVID-CT-MD, COVID-19 computed tomography scan dataset applicable in machine learning and deep learning. *Sci Data* **8**, 121 (2021).
- 11 An, P. *et al.* CT Images in COVID-19 [Data set]. *The Cancer Imaging Archive*, doi:/10.7937/TCIA.2020.GQRY-NC81 (2020).
- 12 Vayá, M. d. I. I. *et al.* Bimcv covid-19+: a large annotated dataset of rx and ct images from covid-19 patients. Preprint at <https://arxiv.org/abs/2006.01174> (2020).
- 13 Morozov, S. P. *et al.* MosMedData: data set of 1110 chest CT scans performed during the COVID-19 epidemic. *Digital Diagnostics* **1**, 49-59 (2020).
- 14 Saltz, J. *et al.* Stony Brook University COVID-19 Positive Cases [Data set]. *The Cancer Imaging Archive*, doi:/10.7937/TCIA.BBAG-2923 (2021).
- 15 Shakouri, S. *et al.* COVID19-CT-dataset: an open-access chest CT image repository of 1000+ patients with confirmed COVID-19 diagnosis. *BMC Research Notes* **14**, doi:/10.1186/s13104-021-05592-x (2021).
- 16 Tsai, E. B. *et al.* The RSNA International COVID-19 Open Radiology Database (RICORD). *Radiology* **299**, E204-E213, doi:10.1148/radiol.2021203957 (2021).
- 17 Roberts, M. *et al.* Common pitfalls and recommendations for using machine learning to detect and prognosticate for COVID-19 using chest radiographs and CT scans. *Nature Machine Intelligence* **3**, 199-217 (2021).
- 18 Medical Imaging and Data Resource Center (MIDRC, 2023); <https://www.midrc.org/>
- 19 DeGrave, A. J., Janizek, J. D. & Lee, S.-I. AI for radiographic COVID-19 detection selects shortcuts over signal. *Nature Machine Intelligence* **3**, 610-619 (2021).
- 20 Driggs, D. *et al.* Machine Learning for COVID-19 Diagnosis and Prognostication: Lessons for Amplifying the Signal While Reducing the Noise. *Radiol Artif Intell* **3**, e210011 (2021).

21 Fricks, R. B. *et al.* Deep learning classification of COVID-19 in chest radiographs: performance and influence of supplemental training. *J Med Imaging (Bellingham)* **8**, 064501 (2021).

22 Sun, J. *et al.* Performance of a Chest Radiograph AI Diagnostic Tool for COVID-19: A Prospective Observational Study. *Radiol Artif Intell* **4**, e210217 (2022).

23 Khemasuwan, D. & Colt, H. G. Applications and challenges of AI-based algorithms in the COVID-19 pandemic. *BMJ Innovations* **7**, 387-398 (2021).

24 Nguyen, D. *et al.* Deep Learning-Based COVID-19 Pneumonia Classification Using Chest CT Images: Model Generalizability. *Front Artif Intell* **4**, 694875 (2021).

25 Abadi, E. *et al.* Virtual clinical trials in medical imaging: a review. *Journal of Medical Imaging* **7**, 042805 (2020).

26 Abadi, E., Paul Segars, W., Chalian, H. & Samei, E. Virtual Imaging Trials for Coronavirus Disease (COVID-19). *AJR Am J Roentgenol* **216**, 362-368 (2021).

27 Abadi, E. *et al.* DukeSim: A Realistic, Rapid, and Scanner-Specific Simulation Framework in Computed Tomography. *IEEE Transactions on Medical Imaging* **38**, 1457-1465 (2019).

28 Tushar, F. I. *et al.* Virtual vs. reality: external validation of COVID-19 classifiers using XCAT phantoms for chest computed tomography. In *Proceeding of the SPIE 12033, Medical Imaging 2022: Computer-Aided Diagnosis*, 1203305 (2022).

29 Dahal, L. *et al.* Virtual versus reality: external validation of COVID-19 classifiers using XCAT phantoms for chest radiography. In *Proceeding of the SPIE 12031, Medical Imaging 2022: Physics of Medical Imaging*, 120310U (2022).

30 Shakouri, S. *et al.* COVID19-CT-dataset: an open-access chest CT image repository of 1000+ patients with confirmed COVID-19 diagnosis. *BMC Res Notes* **14**, 178, doi:/10.1186/s13104-021-05592-x (2021).

31 Li, P. *et al.* A Large-Scale CT and PET/CT Dataset for Lung Cancer Diagnosis (Lung-PET-CT-Dx) [Data set]. *The Cancer Imaging Archive*, doi:/10.7937/TCIA.2020.NNC2-0461 (2020).

32 Wang, L., Lin, Z. Q. & Wong, A. COVID-Net: a tailored deep convolutional neural network design for detection of COVID-19 cases from chest X-ray images. *Sci Rep* **10**, 19549, doi:/10.1038/s41598-020-76550-z (2020).

33 Kiser, K. J. *et al.* Data from the Thoracic Volume and Pleural Effusion Segmentations in Diseased Lungs for Benchmarking Chest CT Processing Pipelines PleThora) [Data set]. *The Cancer Imaging Archive*, doi:/10.7937/tcia.2020.6c7y-gq39 (2020).

34 Armato, S. G. *et al.* The Lung Image Database Consortium (LIDC) and Image Database Resource Initiative (IDRI): A completed reference database of lung nodules on CT scans. *Medical Physics* **38**, 915-931 (2011).

35 RSNA pneumonia detection challenge (2019); <https://www.kaggle.com/c/rsna-pneumonia-detection-challenge/data>

36 Tushar, F. I. *et al.* Classification of Multiple Diseases on Body CT Scans Using Weakly Supervised Deep Learning. *Radiology: Artificial Intelligence* **4**, e210026 (2022).

37 Tushar, F. I., D'Anniballe, V., Rubin, G., Samei, E. & Lo, J. *Co-occurring diseases heavily influence the performance of weakly supervised learning models for classification of chest CT*. In *Proceeding of the SPIE 12033, Medical Imaging 2022: Computer-Aided Diagnosis*, 120332J (2022).

38 Tan, M. & Le, Q. Efficientnetv2: Smaller models and faster training. In *Proceeding of the International Conference on Machine Learning*, 10096-10106 (2021).

39 Robin, X. *et al.* pROC: an open-source package for R and S+ to analyze and compare ROC curves. *BMC Bioinformatics* **12**, 77 (2011).

40 Zhang, Y., Li, X., Segars, W. P. & Samei, E. Comparison of patient specific dose metrics between chest radiography, tomosynthesis, and CT for adult patients of wide ranging body habitus. *Medical Physics* **41**, 023901 (2014).

41 Fujita, M. *et al.* Lung cancer screening with ultra-low dose CT using full iterative reconstruction. *Japanese Journal of Radiology* **35**, 179-189 (2017).

42 Dhont, J., Wolfs, C. & Verhaegen, F. Automatic coronavirus disease 2019 diagnosis based on chest radiography and deep learning - Success story or dataset bias? *Med Phys* **49**, 978-987 (2022).

43 Seyyed-Kalantari, L., Liu, G., McDermott, M., Chen, I. Y. & Ghassemi, M. CheXclusion: Fairness gaps in deep chest X-ray classifiers. In *Proceedings of the Pacific Symposium, BIOCOMPUTING 2021: World Scientific*, 232-243 (2020).

44 Seyyed-Kalantari, L., Zhang, H., McDermott, M. B. A., Chen, I. Y. & Ghassemi, M. Underdiagnosis bias of artificial intelligence algorithms applied to chest radiographs in under-served patient populations. *Nat Med* **27**, 2176-2182 (2021).

45 Willemin, M. J. *et al.* Preparing Medical Imaging Data for Machine Learning. *Radiology* **295**, 4-15 (2020).

46 He, K., Zhang, X., Ren, S. & Sun, J. Deep residual learning for image recognition. In *Proceedings of the IEEE conference on computer vision and pattern recognition*, 770-778 (2016).

47 He, T. *et al.* Bag of tricks for image classification with convolutional neural networks. In *Proceedings of the IEEE/CVF Conference on Computer Vision and Pattern Recognition*, 558-567 (2019).

Supplements:

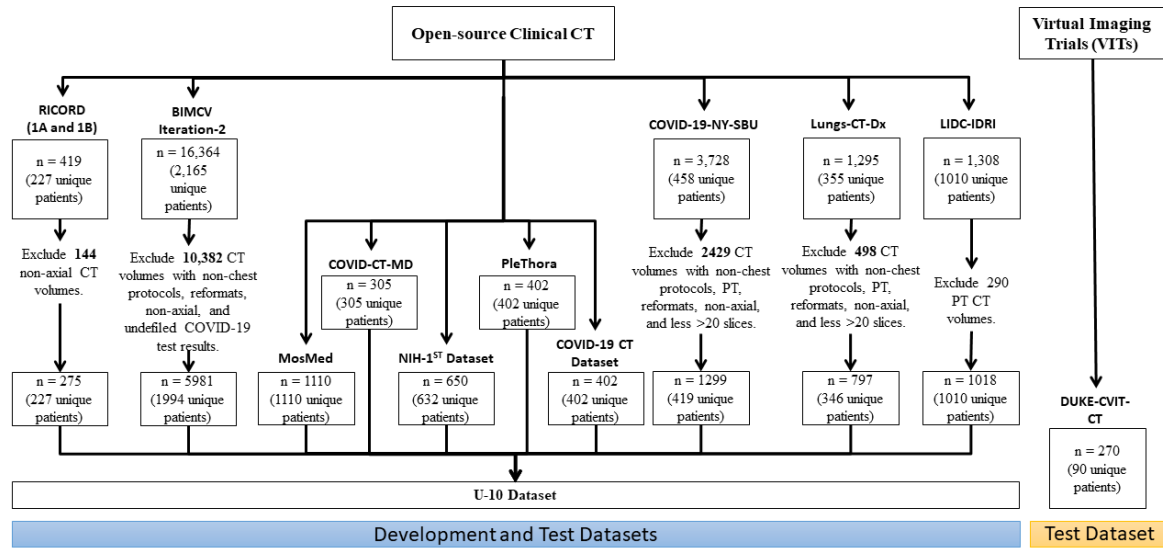


Figure S1. Flowchart of inclusion and exclusion criteria for the chest CT scans. n= number of CT volumes. A total of 16,949 CT scans of 11,166 patients were used for model development and testing. There were ten clinical datasets: RICORD,¹ MosMed,² BIMCV-COVID-19 +/- (BIMCV-V2),³ COVID-CT-MD,⁴ CT Images in COVID-19,⁵ PleThora,⁶ COVID19-CT-dataset,⁷ Stony Brook University COVID-19 Positive Cases (COVID-19-NY-SBU),⁸ A Large-Scale CT and PET/CT Dataset for Lung Cancer Diagnosis (Lungs-CT-Dx),⁹ and Lung Image Database Consortium / Image Database Resource Initiative (LIDC-IDRI).¹⁰ These ten clinical datasets were united into the U-10 CT Dataset. Additionally, simulated data were from the Center for Virtual Imaging Trials CT Dataset, Duke-CVIT-CT.¹¹

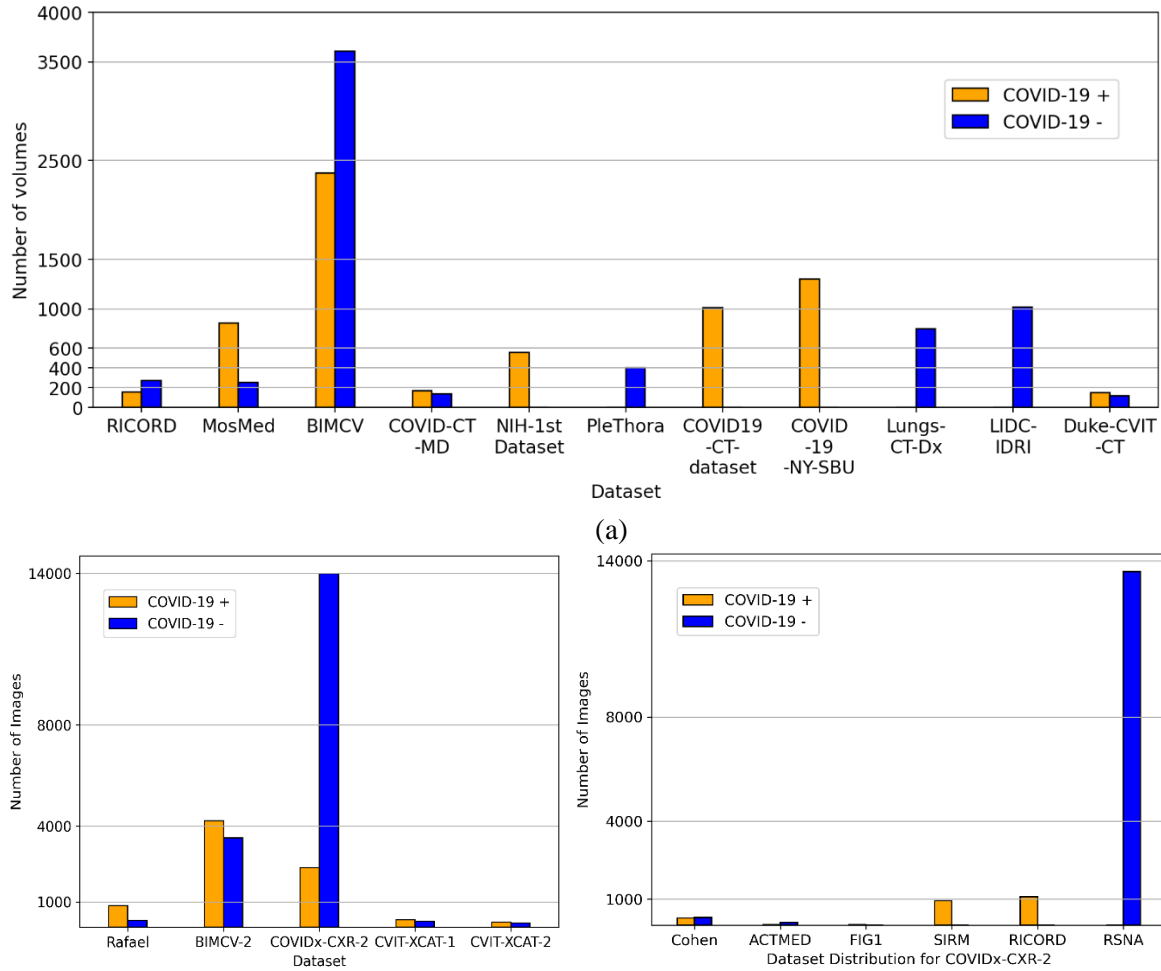


Figure S2: Histograms showing distribution of COVID-19 positive (+) and negative (-) cases among different datasets (clinical and simulated) (a) CTs and (b) CXRs. In the latter, COVID-CXR-2 is further decomposed into its subsets. Log scale is used to show the large variation in numbers of exams. Note that the prevalence varies greatly, and some datasets contain only one class.

Table. S1: Attributes of CT and CXR datasets. Note that simulated data are the only ones that contain all attributes, including the advanced features where the same virtual patient can be imaged with both CT and CXR at multiple doses, with multiple CXR post-processing. X= available.

Datasets	Class Type		Label Level			Advanced features
	COVID-19 positive	COVID-19 negative	Patient-level	Slice-level	Pixel-level	
CT datasets						
RICORD ¹	X	X	X			
MosMed ²	X	X	X			
BIMCV-Iteration 2 ³	X	X	X			
COVID-CT-MD ⁴	X	X	X	X		
An et al. dataset ⁵	X		X			
COVID19-CT-dataset ⁷	X		X			
COVID-19-NY-SBU ⁸	X		X			
Lungs-CT-Dx ⁹		X	X			
LIDC-IDRI ¹⁰		X	X			
Duke-CVIT-CT	X	X	X	X	X	X
CXR datasets						
Fricks <i>et al.</i> dataset ¹²	X	X	X	N/A		
BIMCV-2 ³	X	X	X	N/A		
COVIDx-CXR-2 ¹³	X	X	X	N/A		
Duke-CVIT-CXR	X	X	X	N/A	X	X

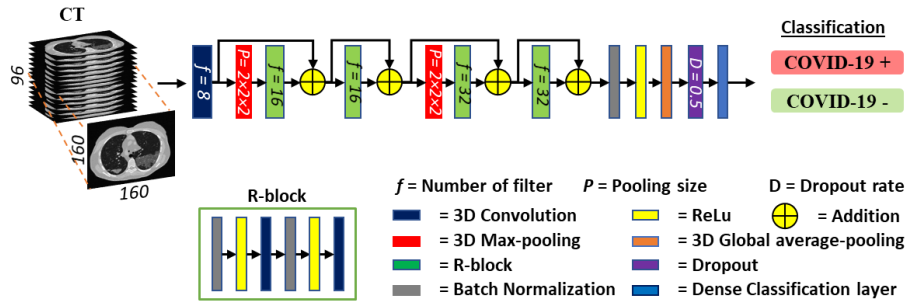


Figure S3- 3D CNN architecture for CT classification of COVID-19. The classification module is a 3D Resnet-like model with 2 R-Blocks in each resolution. The number of filters is denoted as f . The final output is a tensor of the probability of being COVID-19 positive or negative.

References:

- 1 Tsai, E. B. *et al.* The RSNA International COVID-19 Open Radiology Database (RICORD). *Radiology* **299**, E204-E213, doi:/10.1148/radiol.2021203957 (2021).
- 2 Morozov, S. P. *et al.* MosMedData: data set of 1110 chest CT scans performed during the COVID-19 epidemic. *Digital Diagnostics* **1**, 49-59 (2020).
- 3 Vayá, M. d. I. I. *et al.* Bimcv covid-19+: a large annotated dataset of rx and ct images from covid-19 patients. Preprint at <https://arxiv.org/abs/2006.01174> (2020).
- 4 Afshar, P. *et al.* COVID-CT-MD, COVID-19 computed tomography scan dataset applicable in machine learning and deep learning. *Sci Data* **8**, 121, doi:/10.1038/s41597-021-00900-3 (2021).
- 5 An, P. *et al.* CT Images in COVID-19 [Data set]. *The Cancer Imaging Archive*, doi:/10.7937/TCIA.2020.GQRY-NC81 (2020).
- 6 Kiser, K. J. *et al.* Data from the Thoracic Volume and Pleural Effusion Segmentations in Diseased Lungs for Benchmarking Chest CT Processing Pipelines PleThora) [Data set]. *The Cancer Imaging Archive*, doi:/10.7937/tcia.2020.6c7y-gq39 (2020).
- 7 Shakouri, S. *et al.* COVID19-CT-dataset: an open-access chest CT image repository of 1000+ patients with confirmed COVID-19 diagnosis. *BMC Res Notes* **14**, 178, doi:/10.1186/s13104-021-05592-x (2021).
- 8 Saltz, J. *et al.* Stony Brook University COVID-19 Positive Cases [Data set]. *The Cancer Imaging Archive*, doi:/10.7937/TCIA.BBAG-2923 (2021).
- 9 Li, P. *et al.* A Large-Scale CT and PET/CT Dataset for Lung Cancer Diagnosis (Lung-PET-CT-Dx) [Data set]. *The Cancer Imaging Archive*, doi:/10.7937/TCIA.2020.NNC2-0461 (2020).
- 10 Armato, S. G. *et al.* The Lung Image Database Consortium (LIDC) and Image Database Resource Initiative (IDRI): A completed reference database of lung nodules on CT scans. *Medical Physics* **38**, 915-931, doi:10.1118/1.3528204 (2011).
- 11 Abadi, E., Paul Segars, W., Chalian, H. & Samei, E. Virtual Imaging Trials for Coronavirus Disease (COVID-19). *AJR Am J Roentgenol* **216**, 362-368, doi:/10.2214/AJR.20.23429 (2021).
- 12 Fricks, R. B. *et al.* Deep learning classification of COVID-19 in chest radiographs: performance and influence of supplemental training. *J Med Imaging (Bellingham)* **8**, 064501, doi:10.1117/1.JMI.8.6.064501 (2021).
- 13 Wang, L., Lin, Z. Q. & Wong, A. COVID-Net: a tailored deep convolutional neural network design for detection of COVID-19 cases from chest X-ray images. *Sci Rep* **10**, 19549, doi:/10.1038/s41598-020-76550-z (2020).